Monthly Notices of the ROYAL ASTRONOMICAL SOCIETY

MNRAS **525,** 2509–2518 (2023) https://doi.org/10.1093/mnras/stad2414
Advance Access publication 2023 August 25

Sub-second infrared variability from the archetypal accreting neutron star 4U 1728−34

F. M. Vincentelli [1,2]★ P. Casella,[3] A. Borghese [1,2] Y. Cavecchi [4] G. Mastroserio,[5] L. Stella [3] D. Altamirano,[6] M. Armas Padilla [1,2] M. C. Baglio,[7,8] T. M. Belloni [8] J. Casares [1,2] V. A. Cúneo [1,2] N. Degenaar,[9] M. Díaz Trigo,[10] R. Fender,[11] T. Maccarone,[12] J. Malzac,[13] D. Mata Sánchez,[1,2] M. Middleton,[6] S. Migliari,[14,15] T. Muñoz-Darias [1,2] K. O'Brien,[16] G. Panizo-Espinar,[1,2] J. Sánchez-Sierras [1,2] D. M. Russell [7] and P. Uttley[9]

[1]*Instituto de Astrofísica de Canarias, E-38205 La Laguna, Tenerife, Spain*
[2]*Departamento de Astrofísica, Universidad de La Laguna, E-38206 La Laguna, Tenerife, Spain*
[3]*INAF – Osservatorio Astronomico di Roma, Via Frascati 33, I-00078 Monteporzio Catone, Italy*
[4]*Departament de Física, EEBE, Universitat Politècnica de Catalunya, Calle Eduard Maristany, 10 E-08930 Barcelona, Spain*
[5]*INAF – Osservatorio Astronomico di Cagliari, via della Scienza 5, I-09047 Selargius Cagliari, Italy*
[6]*Department of Physics and Astronomy, University of Southampton, Southampton, Hampshire SO17 1BJ, UK*
[7]*Center for Astro, Particle and Planetary Physics, New York University Abu Dhabi, PO Box 129188, Abu Dhabi, UAE*
[8]*INAF - Osservatorio Astronomico di Brera, Via E. Bianchi 46, I-23807 Merate, Italy*
[9]*Anton Pannekoek Institute for Astronomy, University of Amsterdam, Science Park 904, 1098 XH Amsterdam, The Netherlands*
[10]*ESO, Karl-Schwarzschild-Strasse 2, D-85748 Garching bei München, Germany*
[11]*Astrophysics, Department of Physics, University of Oxford, Denys Wilkinson Building, Keble Road, Oxford OX1 3RH, UK*
[12]*Department of Physics and Astronomy, Texas Tech University, Lubbock, TX 79409-1051, USA*
[13]*IRAP, Universite' de Toulouse, CNRS, UPS, CNES, Toulouse, France*
[14]*XMM–Newton Science Operation Center, ESAC/ESA, Camino Bajo del Castillo s/n, Urb. Villafranca del Castillo, E-28691 Villanueva de la Cañada, Madrid, Spain*
[15]*Institute of Cosmos Sciences, University of Barcelona, Martí i Franquès 1, 08028 Barcelona, Spain*
[16]*Department of Physics, Durham University, South Road, Durham, DH1 3LE, UK*

Accepted 2023 August 2. Received 2023 July 20; in original form 2023 May 30

ABSTRACT

We report on the first simultaneous high-time resolution X-ray and infrared (IR) observations of a neutron star low mass X-ray binary in its hard state. We performed ≈ 2 h of simultaneous observations of 4U 1728−34 using HAWK-I@VLT, *XMM–Newton*, and *NuSTAR*. The source displayed significant X-ray and IR variability down to sub-second time-scales. By measuring the cross-correlation function between the IR and X-ray lightcurves, we discovered a significant correlation with an IR lead of ≈ 30–40 ms with respect to the X-rays. We analysed the X-ray energy dependence of the lag, finding a marginal increase towards higher energies. Given the sign of the lag, we interpret this as possible evidence of Comptonization from external seed photons. We discuss the origin of the IR seed photons in terms of cyclo-synchrotron radiation from an extended hot flow. Finally, we also observed the IR counterpart of a type-I X-ray burst, with a delay of ≈ 7.2 s. Although some additional effects may be at play, by assuming that this lag is due to light travel time between the central object and the companion star, we find that 4U 1728−34 must have an orbital period longer than 3 h and an inclination higher than 8°.

Key words: accretion, accretion discs – stars: neutron – X-rays: binaries.

1 INTRODUCTION

Low mass X-ray binaries (LMXBs) are systems in which a neutron star (NS) or a black hole (BH) is accreting mass from a small mass companion star. During their outbursts, they display a broad and complex spectral energy distribution which varies during different stages of their activity. Two main states can be identified as (see e.g. Tananbaum et al. 1972; Fender, Belloni & Gallo 2004; Migliari & Fender 2006; Done, Gierliński & Kubota 2007; Lin, Remillard & Homan 2007; Belloni, Motta & Muñoz-Darias 2011; Muñoz-Darias et al. 2014): a so-called 'soft state', in which the emission is mainly thermal, arising from an optically thick, geometrically thin accretion disc (dominating the soft X-ray part of the spectrum); and a 'hard state', in which the X-ray spectrum is dominated by a cut-offed power law, with a typical cut-off value of ≈ 10–20 keV for NSs and ≈ 100 keV for BHs (Burke, Gilfanov & Sunyaev 2017). This component is explained in terms of a geometrically thick, optically thin inflow (also referred to as 'corona'), which Comptonizes softer X-ray photons arising from the disc (in BH; Zdziarski & Gierliński

★ E-mail: vincentelli.astro@gmail.com

2004; Done et al. 2007) or the boundary layer (in NS; Lin et al. 2007). In the hard state, these systems can also show a flat spectrum which extends from radio to optical–infrared wavelengths, usually associated with synchrotron radiation from a compact jet (see e.g. Corbel & Fender 2002; Russell, Fender & Jonker 2007; Migliari et al. 2010; Baglio et al. 2016; Díaz Trigo et al. 2018; Tetarenko et al. 2021).

It is generally accepted that the geometry of the accretion flow around accreting compact objects evolves during their outbursts (see e.g. Esin, McClintock & Narayan 1997; Lin et al. 2007, 2009; Ingram & Done 2010; De Marco et al. 2017; Wang et al. 2017, 2019; van den Eijnden et al. 2020; Méndez et al. 2022). However, the exact structure of the inflow and its connection to the jet is still a matter of debate (Kalemci, Kara & Tomsick 2022). A fundamental property of LMXBs that can help answering these key questions is the presence, during the hard state, of strong stochastic variability across the electromagnetic spectrum down to sub-second time-scales (see e.g. Motch, Ilovaisky & Chevalier 1982; van der Klis 1994; Belloni et al. 2005; Tetarenko et al. 2021).

The ultraviolet/optical/infrared (UV/O/IR) range contains contributions from three emitting components that vary along the outburst and act on different time-scales: irradiated disc, jet, and contribution from an extended hot inflow (Corbel & Fender 2002; Hynes 2005; Gierliński, Done & Page 2009; Migliari et al. 2010; Chaty, Dubus & Raichoor 2011; Buxton et al. 2012; Corbel et al. 2013; Poutanen, Veledina & Revnivtsev 2014; Kosenkov et al. 2020). Thus, variability studies in these bands have proved to be extremely powerful to constrain the properties of LMXBs.

In recent years, the development of new fast O-IR photometers has allowed for a rapid growth of strictly simultaneous high-time resolution multiwavelength observations of BH LMXBs. The discovery of $\approx +0.1$ s lag in at least three BHs (GX 339-4, V404 Cyg, and MAXI J1820+070) between X-ray and the O-IR emission clearly showed that mass accretion rate fluctuations can travel from the inflow to the jet, where they are re-emitted as synchrotron radiation (Casella et al. 2010; Gandhi et al. 2010; Malzac 2014; Gandhi et al. 2017; Paice et al. 2019). This opened a new window in jet physics studies, providing new fundamental constraints on the jet speed (Casella et al. 2010; Tetarenko et al. 2018; Zdziarski, Tetarenko & Sikora 2022), the height and extension of the first shock region (Gandhi et al. 2017; Vincentelli et al. 2018; Paice et al. 2019) and the launching radius (Vincentelli et al. 2019).

Further observations lead to the discovery of a non-linear correlation between the two bands (Kanbach et al. 2001; Durant et al. 2011; Veledina et al. 2017; Paice et al. 2021; Vincentelli et al. 2021), as well as O-IR quasi-periodic oscillations (Motch et al. 1983; Kalamkar et al. 2016; Vincentelli et al. 2019, 2021). This indicated the contribution of more than one variable component to the O-IR emission (as also suggested by long term O-IR studies; Kosenkov et al. 2020). One of the most promising candidates to explain these intriguing features is synchrotron radiation from the external regions of a hot magnetized inflow (Veledina, Poutanen & Vurm 2011). Few LMXBs, including both BH and NS, have shown possible evidence of this component, but it is not clear under which conditions it can dominate over the jet (Degenaar et al. 2014; Veledina et al. 2017; Paice et al. 2021; Shahbaz et al. 2023).

Despite the richness of O-IR phenomenology in BH LMXBs, relatively few studies focused on the fast multiwavelength properties of NS LMXBs, mainly because of their lower luminosity.[1] Due to their strong flaring and non-stationary variability, most of the attention focused on objects persistently accreting at high rates (i.e. the so-called 'Z sources'; McGowan et al. 2003; Dubus et al. 2004; Durant et al. 2011; Shahbaz et al. 2023; Vincentelli et al. 2023), or transitional millisecond pulsars (Shahbaz et al. 2015, 2018; Baglio et al. 2019; Papitto et al. 2019; Baglio et al. 2023). Yet, no study has been done for NS LMXBs in their 'canonical' hard state.

Here, we present the first simultaneous fast IR/X-ray observation of the accreting NS 4U 1728−34 (or GX 354−0, RA: 17 31 57.73, Dec. : −33 50 02.5) during its hard state. This system is a well-known weakly magnetized NS inferred to accrete from a H-poor donor (Shaposhnikov, Titarchuk & Haberl 2003; Galloway et al. 2010). It is classified as a persistent atoll-type LMXB with high Galactic hydrogen column density, $N_{\rm H} = 2.4 - 4.5 \times 10^{22}\,{\rm cm}^{-2}$ (Piraino, Santangelo & Kaaret 2000; D'Aí et al. 2006; Díaz Trigo et al. 2018). Atoll-type systems are X-ray sources which can undergo transitions between a soft and a hard state. When they do, they trace typical tracks in the X-ray colour–colour diagram (i.e. the so called "Island" and "Banana" branches), associated also to an evolution of timing properties (see, e.g. Hasinger & van der Klis 1989; van der Klis 2006). As observed in BH LMXBs, the broad-band noise components of the X-ray power spectrum, along with its quasi-periodic oscillations, evolve towards high frequencies as the source approaches a softer, higher luminosity phase (see e.g. Psaltis, Belloni & van der Klis 1999; Homan et al. 2007; Altamirano et al. 2008). While the duration of these state can vary significantly from source to source (see e.g. van der Klis 2006; Muñoz-Darias et al. 2014, and references therein), 4U 1728−34 undergoes regular state transitions every ∼40–60 d (Muñoz-Darias et al. 2014; for previous detection of these periodicities see also: Kong, Charles & Kuulkers 1998; Galloway et al. 2003)

Recent X-ray/IR observations in the soft state have detected the first infrared counterpart of a type-I burst (Vincentelli et al. 2020). These rapid X-ray flashes of light arise from a thermonuclear runway on the surface of the NS (Hansen & van Horn 1975; Woosley & Taam 1976). The low energy counterpart (detected at UV/O/IR wavelengths) of these events is usually associated to the reprocessed emission from the disc and the companion star. Thus, the delay between the X-ray and the UV/O/IR emission can be used to constrain the orbital parameters of these systems (see e.g. Hynes et al. 2006; Muñoz-Darias et al. 2007; Vincentelli et al. 2020).

2 DATA

2.1 Infrared: HAWK-I@VLT

We performed high time-resolution photometric observations of 4U 1728−34 with HAWK-I (Pirard et al. 2004), mounted at the UT4 at the Very Large Telescope in Cerro Paranal, Chile. Observations were carried out on the 2019-03-23 (MJD 58565) between 06:34 and 08:34 UTC in FastPhot mode (program ID: 0102.D-0182) using a window of 128 × 64 bins, allowing us to reach a time resolution of 0.125 s. Data were recorded in $N = 200$ data cubes of 250 frames each, separated by ≈ 3 s gaps. We then measured the back ground subtracted lightcurve from the target, a bright reference and a comparison star using the ULTRACAM software (Dhillon et al. 2007). In order not to lose the tracking of the stars, the relative position of the target and comparison star was fixed with respect to the reference star. Within one cube the position of the aperture was able to tweak its position, following

[1]The average X-ray peak luminosity of BH LMXBs is $\approx 7 \times 10^{37}\,{\rm erg\,s^{-1}}$ against the $\approx 3.8 \times 10^{37}\,{\rm erg\,s^{-1}}$ NS LMXBs (Yan & Yu 2015). Furthermore, stellar mass BHs are also brighter at O-IR wavelengths ($L_{O\text{–}IR,BH} \approx \times 10^{34}\,{\rm erg\,s^{-1}}$, against $L_{O\text{–}IR,NS} \approx \times 10^{33}\,{\rm erg\,s^{-1}}$; Russell et al. 2006).

the stars. One set of aperture radii of the extraction was defined for each cube in order to take into account long term seeing variations. To remove any additional spurious effects, we then normalized the target lightcurve to the reference star (VVV J173159.32-335001.92, $K_s = 10.562 \pm 0.001$). The lightcurve extracted from a nearby comparison star (VVV J173200.33-335005.87, $K_s = 14.58 \pm 0.04$) showed a stable lightcurve without long term trends. The average magnitude of 4U 1728−34 was 14.5 ± 0.02 (≈ 1.1 mJy, a similar flux to past measurements by Díaz Trigo et al. 2018). A fraction of the cubes suffered from a few frame losses. Therefore, when considering the cross-correlation with the X-rays, these cubes were discarded from the analysis. During a few cubes, the source ended up too close to the edge of the detector, distorting the obtained lightcurve: also these cubes were excluded from the overall analysis. After extracting the lightcurve, we put the times stamps in the Dynamical Barycentric Time system using the JPL DE405 Earth ephemerides adopting the method described in Eastman, Siverd & Gaudi (2010).

2.2 Soft X-rays: *XMM–Newton*

We observed 4U 1728−34 with the EPIC-pn camera onboard of the X-ray (0.5–10 keV) telescope *XMM–Newton* in Timing mode (Strüder et al. 2001). Observations were carried out on the same night between 05:37 and 13:32 UTC (OBSID: 0831791401). After applying the barycentric correction (through the BARYCEN tool adopting the JPL DE405 Earth ephemeris), we extracted the events between column RAWX 27 and 47, selecting only events with PATTERN <= 4 and FLAG == 0. The data also show a clear X-ray burst during the HAWK-I time window: for the analysis of the stochastic variability (and the correlation with the IR fast variability, see Section 3.1 and 3.2), this feature was discarded from the data. We excluded events in a window between 4200 and 4400 s from the beginning of the observation. The selected X-ray events were binned to the IR lightcurve. Due to the very high count rate of this event, which distorts the shape of the lightcurve, for the analysis of the burst signal (see Section 3.3) we obtained the lightcurve using the command EPICLCCORR with 0.5 s time resolution.

2.3 Hard X-rays: NuSTAR

NuSTAR (Harrison et al. 2013) observed 4U 1728−34 from the 2019-03-22 22:26:09 to 2019-03-23 12:11:09 UTC for a total on-source exposure time of 19.3 ks (OBSID: 90501312002) with both focal plane module A and B (FPMA and FPMB, hereafter). We processed the event lists, filtered photons between 3 and 79 keV, excluded the passages of the satellite through the South Atlantic Anomaly using the tool `nupipeline`. Barycentric correction was also applied through the FTOOL command BARYOCRR (also in this case we used JPL DE405 Earth ephemeris). Both source and background counts were accumulated within a circular region of radius 150 arcsec. We then extracted the barycenter source light curves for both FPMs and inspected them for the presence of bursts. We detected one burst with a duration ≈ 100 s before the strictly simultaneous *XMM–Newton*/HAWK-I campaign. The burst detected in the *XMM–Newton*/HAWK-I campaign, instead, took place during a visibility gap. After excluding the identified burst, spectra and response files were generated applying the script `nuproducts`. We binned the spectra to obtain at least a signal-to-noise ratio of 20.

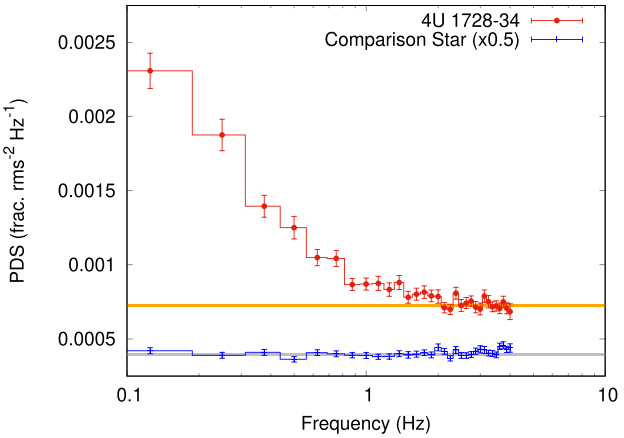

Figure 1. IR PDS of our target (4U 1728−34; red points) and the chosen comparison star (blue points). While the former shows clear red noise, the latter is consistent with Poissonian noise. The comparison star PDS has been rescaled for clarity. The grey line represents a constant fit to the comparison star PDS, while the orange line represents the best constant fit in the range between 3 and 4 Hz.

3 DATA ANALYSIS AND RESULTS

3.1 Stochastic variability

Thanks to HAWK-I's sub-second time resolution we measured the power density spectrum (PDS) in the IR band using the recipe described by Uttley et al. (2014). We first investigated if the target was significantly variable computing the PDS with 64 bins (i.e. segment length = 8 s) per segment for both our target and the comparison star (see Fig. 1). While the first shows clear red noise, typically observed in accreting systems (see e.g. Press 1978; Uttley, McHardy & Vaughan 2005; Scaringi et al. 2015, and references therein), the latter shows a flat spectrum, consistent with just uncorrelated noise. Some deviations from the constant are seen (see e.g. around 2 and 4 Hz). We note, however, that they lie within $2\,\sigma$ from our constant best fit, and thus they are unlikely due to instrumental artefacts that could affect the signal.

We then computed a PDS with a better frequency resolution and coverage (i.e. going at lower frequencies): to do this we filled the gaps by adding log-normally distributed points which kept the same flux, and high frequency PDS of our IR lightcurve. The PDS was computed using 128 bins per segment (i.e. segment length = 16 s) and a geometrical rebinning of 1.2 (see Fig. 2). While at low frequencies the PDS shows a break around 0.3 Hz, it shows an upturn above $\approx$1 Hz. Given the trend at frequencies below 1 Hz, such a change in slope is unlikely to be only aliasing. However, such an effect could be caused by an underestimation of the white noise level, which was computed following the recipe in Vaughan et al. (2003). Thus, we also computed the PDS by estimating the noise by fitting the constant level between 3 and 4 Hz. Although this represents the most conservative estimate, we still measure significant variability above 1 Hz (yellow empty points in Fig. 2). The integrated rms computed in the former case is ≈ 2 per cent.

We compared the IR PDS to the PDS of the *XMM–Newton* data with 16 348 bins per segment and a geometrical rebinning factor of 1.1. The X-ray PDS shows strong broad-band noise as typically observed in NS LMXBs in their hard state, with a peak (in νP_ν units) at around few Hz and an integrated rms of 20 per cent. This value is consistent with typical expectations from the hard state (Muñoz-Darias et al. 2014).

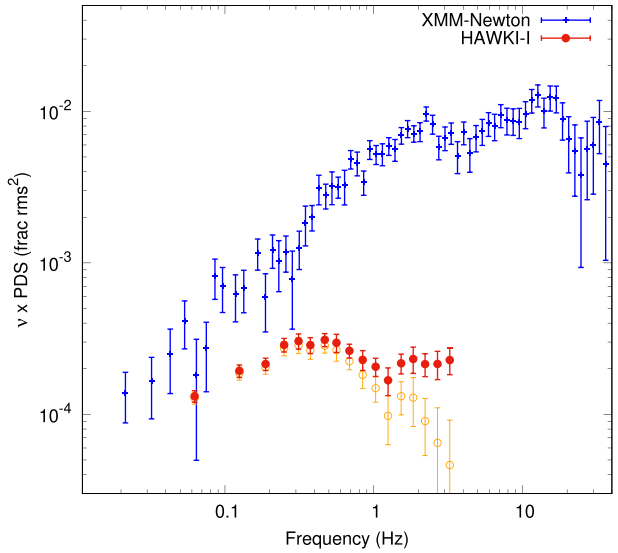

Figure 2. X-ray (blue points) and IR (red filled points) noise-subtracted PDS (in νP_ν units) of 4U 1728−34 during our observations. The yellow empty circles represent the IR PDS estimating the Poissonian noise fitting a constant between 3 and 4 Hz (see orange line in Fig. 1). The IR PDS has significantly lower variability and shows a break at lower frequencies.

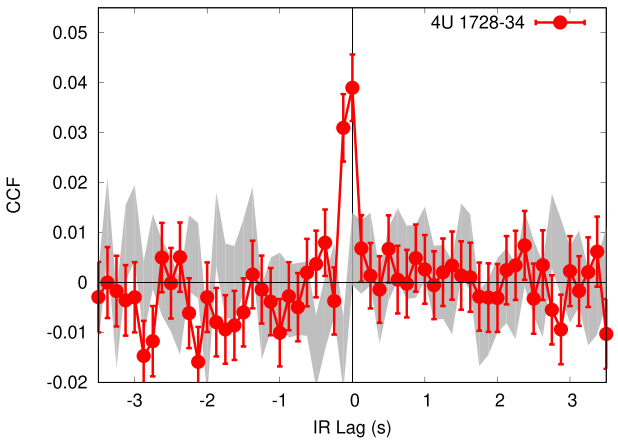

Figure 3. CCF computed between *XMM–Newton* and HAWK-I for 4U 1728−34 (red points) and the comparison star (grey curve).

We characterized the origin of this noise by measuring the discrete cross-correlation function (CCF) between the X-ray (0.5–10 keV) and IR using the same procedure described by Gandhi et al. (2010). As in all previous studies, we use the X-ray as a reference band: i.e. positive lag implies that the IR lags the X-rays. All plots follow this convention, unless specified otherwise. The *XMM–Newton*/HAWK-I CCF has a poorly resolved peak around ≈0, which seems to be slightly asymmetric around negative lags (Fig. 3). By computing the lag as the weighted average of the cross-correlation lags between ±0.5 s and propagating the errors accordingly, we obtain a lag of -41 ± 11 ms: i.e. IR *leads* the X-ray variability. We compared this value with the Fourier lags: i.e. using the phase of the IR/X-ray cross-spectrum. This was computed following the steps described in Uttley et al. (2014). A comparable value is also obtained when computing the Fourier time lag between the X-ray and IR lightcurves at high frequencies: -32 ± 15 ms in the 1–4 Hz range and -42 ± 20 ms between 2 and 4 Hz.

In order to verify the significance of the observed correlation, we performed two tests. We first evaluated the CCF between *XMM–Newton* and the IR lightcurves of the comparison star: the absence of correlation shown in Fig. 3 (grey curve) demonstrates that the peak is not spurious. Secondly, we checked whether the peak was due to uncorrelated noise fluctuations. To do so, we simulated N = 10^3 synthetic lightcurves with the same PDS of the *XMM–Newton* lightcurve and random phases, and cross-correlated them with the IR lightcurve. From the width of the obtained distribution, we found that our peak is significant at ≈8σ. Finally, we also verified if the shape was affected by counting statistics, correcting the normalization from the excess variance (Vaughan et al. 2003). However, we did not find a significant variation in the shape of the CCF, nor of its inferred lag. Therefore, we can conclude that the asymmetry of the CCF, and thus the IR lead, is real.

3.2 CCF energy dependence

We investigated the CCF energy dependence by using *XMM–Newton* lightcurves extracted in the 0.5–4 and 4–10 keV bands. The resulting plots (see Fig. 4, Top panels) show a possible evolution between the two bands. To exclude that this is an effect due to the normalization, we evaluated the Fourier domain phase lags between the IR and the two X-ray bands by using 64 bins per segment and a geometrical rebinning factor of 1.4. Although the statistics is poor, the bottom panels of Fig. 4 show that the resulting lag-frequency spectra appear to marginally deviate from each other above 1 Hz (where the lag in the 4–10 keV band becomes longer).

In order to investigate further this result, we computed the lag-energy spectrum by integrating the cross-spectrum between 1 and 4 Hz for four X-ray energy bands (0.5–2, 2–4, 4–6, and 6–10 keV). Given the IR lead, we used the IR bands as reference. We caution the reader that this *inverts* the convention used so far: i.e. *positive lag means that the X-rays lag the IR*. The resulting time-lag versus energy-spectrum is shown in Fig. 5. While the IR lead (or X-ray delay) does not evolve significantly between 0.5 and 6 keV, a marginal increase can be seen in the 6–10 keV band. We also attempted to measure the lags using broader bands (0.5–4 and 4–10 keV, i.e. as for the analysis shown in Fig. 4) and we found only a marginal difference of ≈1.5σ: 17 ± 15 to 62 ± 27 ms. We note that, as expected from the lag-frequency spectrum, by performing the same analysis at lower frequencies (i.e. 0.1–1 Hz), all lags are consistent with zero.

3.3 Type-I burst

As mentioned above, the *XMM–Newton* lightcurve presented a clear X-ray burst simultaneous with the HAWK-I cubes. However, due to the presence of stochastic variability, the IR lightcurve does not show a clear excess as in the previous burst reported by Vincentelli et al. (2020). Nonetheless, by measuring the CCF including the burst, we found a broad peak which suggests that the IR does respond to the X-ray burst also in the hard state (see Fig. 6, right panel). Interestingly, the CCF seems also to show a weak anticorrelation at ≈ −5 s. By inspecting the IR lighcurve with lower time resolution, we found the presence of a marginal dip during the initial phase of the burst followed by a positive response to the X-ray burst (see Fig. 6, left panel), which could explain the weak anticorrelation at negative lags. We estimated the significance of this correlation by cross-correlating the XMM lightcurve including the burst with an uncorrelated signal with the same properties of the IR lightcurve. We simulated 10^3 lightcurves with the same signal-to-noise ratio and power spectrum

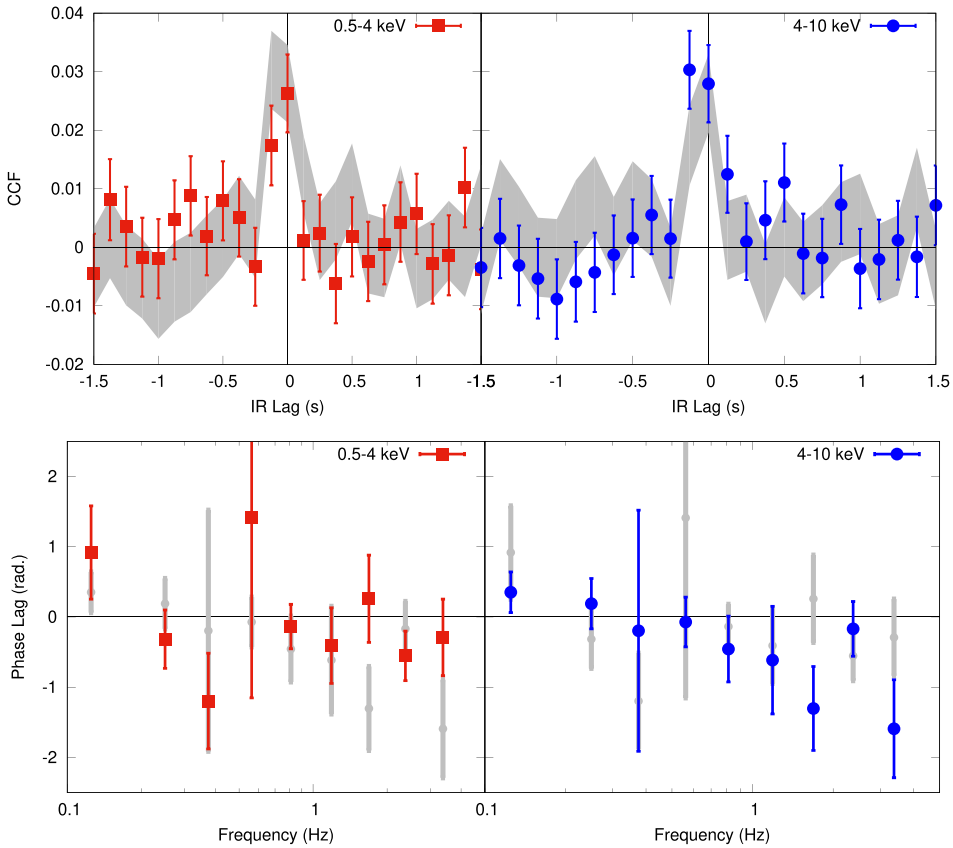

Figure 4. *Top panel*: X-ray/IR CCF using different X-ray energies: 0.5–4 keV (red squares on the left) and 4–10 keV (blue circles on the right). *Bottom panel*: X-ray/IR phase lags using the same bands (and colour code). To ease comparison, on the left panels grey lines represent measurements done with the 4–10 keV band and on the right panels grey lines reproduce the calculations using the 0.5–4 keV band.

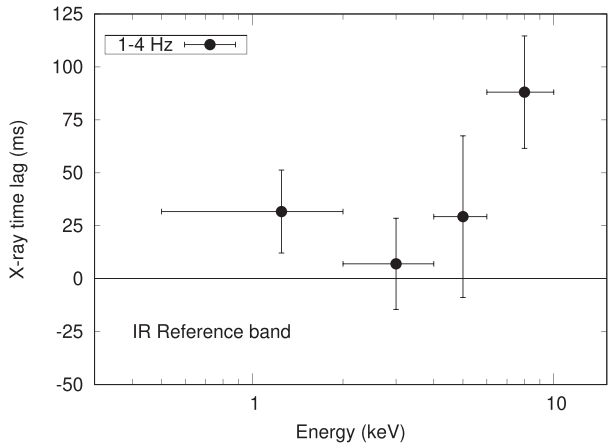

Figure 5. Lag-energy spectrum using the IR as a reference band: i.e. positive lag means X-ray lagging the IR. The plot shows how the lag seems to become larger at energies above 6 keV.

measured by HAWK-I, aligned them to the XMM lightcurve and computed the CCF for all the possible shifts. The $1\,\sigma$ threshold obtained from the distribution is plotted in Fig. 6 (right panel). The peak of the CCF is highly significant ($\approx 4.4\,\sigma$), while, as expected, the dip at negative lag is just around $\approx 3\,\sigma$.

Following the procedure described by Gandhi et al. (2017) and Peterson et al. (1998), we evaluated the X-ray/IR delay through the weighted average (and its standard error) of the CCF within its full width half maximum, finding a lag of 7.2 ± 1.4 s. Past observations in the soft state showed a delay associated to the burst of 4.5 ± 0.25 s (Vincentelli et al. 2020), thus smaller with a $\approx 2\sigma$ confidence level.

3.4 X-ray spectral analysis

We also characterized the X-ray spectral state of the source, by analysing the *NuSTAR* spectrum between 3 and 79 keV (Fig. 7). Following past spectral studies of NS LMXBs (Wang et al. 2017, 2019; Ludlam et al. 2019; van den Eijnden et al. 2020) we used a model with four components: interstellar absorption, a black body component, a cut-off power law, and reflection. In details, we used a Comptonization model (THCOMP; Zdziarski et al. 2020) convoluted with a black body component (BBODYRAD) and a relativistic reflection model (RELXILLCP; García et al. 2014). We fixed the hydrogen column density $N_{\rm H}$ to the value reported in the Heasarc[2] database for the source coordinates, i.e. 1.35×10^{22} cm^{-2}[3]

The model can reproduce with good agreement the data ($\chi^2/dof \approx 1.07$) and the best-fitting values are reported in Table 1. We found

[2]https://heasarc.gsfc.nasa.gov/cgi-bin/Tools/w3nh/w3nh.pl

[3]Past studies have found a better spectral fit by leaving the absorption free, finding $N_{\rm H} \approx 2.5 \times 10^{22}$ cm^{-2} (Piraino et al. 2000; D'Aí et al. 2006; Díaz Trigo et al. 2018). We note that we also performed the analysis with this value and (probably due to the energy band pass) did not find any significant variations in the inferred parameters.

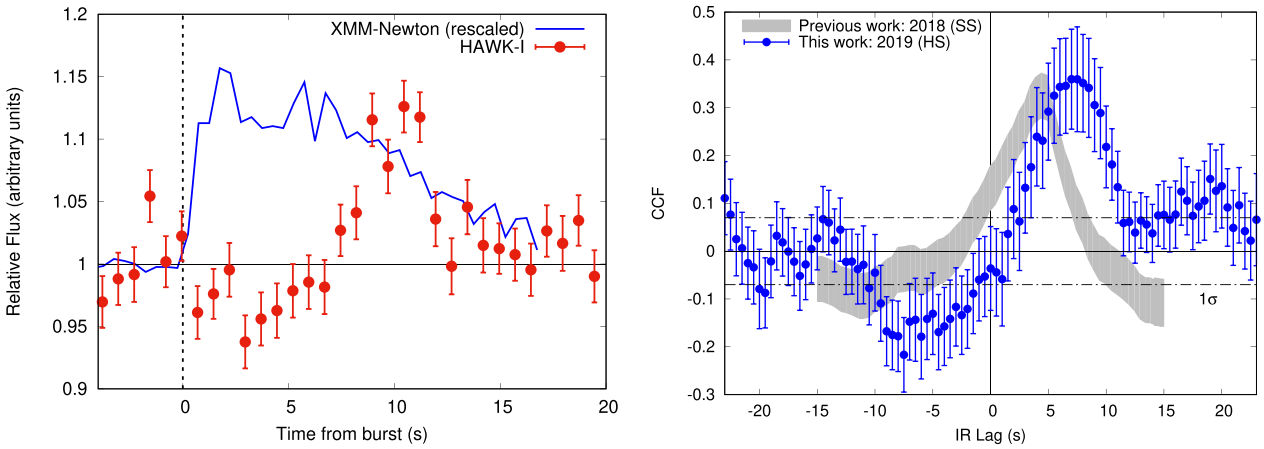

Figure 6. *Left Panel: XMM–Newton* (blue line) and HAWK-I lightcurve (red points, rebinned to 0.75 s for clarity) during the type-I burst. The dashed line was placed at the rise of the burst (i.e. between the first bin with a clear rise, and the last consistent with the persistent). The IR lightcurve shows a marginal anticorrelation around the peak of the X-ray burst followed by a clear rise. The gap at the end of the *XMM–Newton* burst is due to telemetry drop-out. *Right Panel:* CCF of the hard state (HS, blue points) compared with the one measured in the soft state (SS, grey curve; Vincentelli et al. 2020). The latter was computed only up to a lag of ±15 s because of the limited duration of the simultaneous data. Nonetheless, a clear difference between the two epochs is present. The dashed–dotted lines represent the 1σ confidence noise level for the hard state observations.

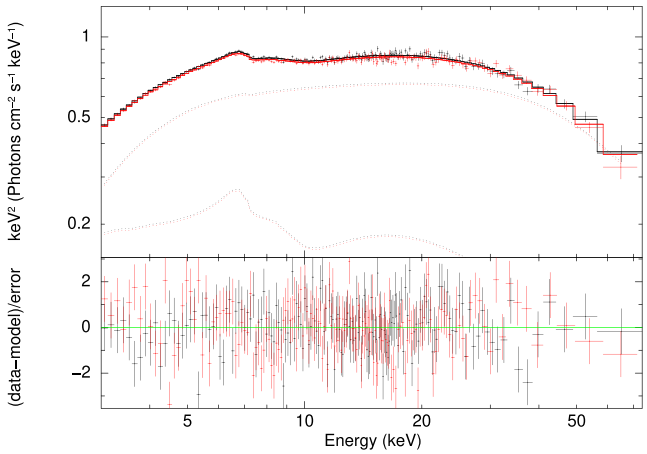

Figure 7. *Top Panel: NuSTAR* spectra of 4U 1728−34. Black and red points represent the data from FPMA and FPMB detectors, respectively. The continuous line represents the overall model, while the dashed lines indicate the individual components. *Bottom Panel:* Residuals of the fit.

the presence of a thermal component at $kT \approx 1$ keV, associated most probably the boundary layer (see e.g. Lin et al. 2007; Armas Padilla et al. 2017). The temperature of the hot Comptonizing medium was found to be $kT_e \approx 15$ keV. Both these values are consistent with past measurements of NS LMXBs X-ray spectra during the hard state (Lin et al. 2007; Burke et al. 2017). The value of the covering fraction is consistent with 1, which indicates that all the seed photons are Comptonized. Regarding the reflection component, the spectrum is consistent with a highly ionized, ($\log \xi \approx 3.5$), truncated ($R_{in} \approx 10^7$ cm) disc with a low inclination (i between ≈20 and 30°). The reflection model allows us to define two disc emissivity profile indices and a radius for the transition between the two indices. Since the fit does not require strong relativistic effects (the disc is truncated), we fixed both indices to 3 which is what is predicted in the Newtonian case. The spin was also fixed to 0, for the same reason. Furthermore, by leaving the density (ρ) of the disc as a free parameter, we find a value of $\rho \approx 2.5 \times 10^{18}$ cm^{-3}.

Table 1. Best-fitting parameters for the *NuSTAR* FPMA + FPMB spectral analysis. The data were well reproduced assuming an absorbed Comptonization model + reflection: specifically, we used the model PHABS × (THCOMP ⊛ BBODYRAD + RELXILLCP). N_H was fixed to 1.35×10^{22} cm^{-2}, $a = 0$ and both emissivity profile indices to 3. All errors are reported with 90 per cent confidence level.

Component	Parameter	Value
THCOMP		
	Γ_τ	1.9 ± 0.01
	kT_e (keV)	$15.4^{+0.3}_{-0.6}$
	cov_{frac}	$0.99^{+0.01}_{-0.09}$
BBODYRAD		
	kT (keV)	$0.96^{+0.07}_{-0.01}$
	norm	154^{+28}_{40}
RELXILLCP		
	inc (°)	23^{+13}_{-9}
	R_{in} ($\times 6$ GM c^{-2})	6^{+9}_{-2}
	logξ	3.5 ± 0.1
	log ρ (cm^{-3})	$18.4^{+0.7}_{-0.5}$
	norm ($\times 10^{-3}$)	1.8 ± 0.4
χ^2 /dof (FMPA)		491/485
χ^2 /dof (FMPB)		546/466
χ^2 /dof (total)		1037/961
Flux 3–79 keV (erg cm^{-2} s^{-1})		3.6×10^{-9}
Flux 3–6 keV (erg cm^{-2} s^{-1})		7.3×10^{-10}
Flux 6–9 keV (erg cm^{-2} s^{-1})		5.5×10^{-10}

As mentioned above, this observation has a much harder spectrum compared to the first burst detection reported in Vincentelli et al. (2020). In particular, the previous observation is dominated by a strong thermal component, which can be fitted with a disc black body emission with a temperature of ≈3 keV. We also find evidence of reflection features as well as a hard tail above 50 keV. This is in line with the previous studies of the source (see e.g. Kajava et al. 2017; Wang et al. 2019), and a more detailed analysis on the evolution of the spectrum, beyond the aim of this paper, is ongoing (Vincentelli et al., in preperation).

4 DISCUSSION

4.1 Stochastic variability and lags

Our strictly simultaneous *XMM–Newton*/HAWK-I observations of 4U 1728−34 show a strong correlated signal with an infrared lead of ≈ 40 ms. Given that the CCF structure is unresolved, it is not straightforward to give a physical explanation to this delay. It is the first time that the sub-second IR domain is explored for a weakly magnetized NS LMXB in the hard state and there are currently no models which can predict this feature. Given the similarity between BH LMXBs and these systems (see e.g. Psaltis et al. 1999; Muñoz-Darias et al. 2014; Vincentelli et al. 2023), we attempted to interpret this signal through models recently developed for stellar mass BHs.

Historically, broad-band spectral studies of LMXBs have usually interpreted the presence of an IR excess in the hard state as a jet component (Corbel & Fender 2002; Russell et al. 2006; Migliari et al. 2010; Gandhi et al. 2011; Corbel et al. 2013; Baglio et al. 2016; Díaz Trigo et al. 2018; Marino et al. 2020). From a timing point of view, this scenario has been confirmed only for BH LMXBs thanks to the detection of a 0.1 s lag between the X-ray and O-IR variability (Gandhi et al. 2008; Casella et al. 2010; Malzac 2014). According to this model, accretion-rate fluctuations from the inflow (which are observed in X-rays) are injected in the jet, where they are re-emitted in the form of synchrotron radiation at lower energies (from O-IR to radio) through the collisions of internal shocks (Jamil, Fender & Kaiser 2010; Malzac 2013): therefore the IR responds to the variations in X-rays with a positive lag.

The IR lead found in our analysis seems to disfavour a pure jet model. However, it is important to recall that due to the poor resolution of the CCF, we cannot rule out completely the presence of a jet. A component with a (positive) lag, smaller than half the time resolution of our CCF, could still be present. On this regard, it is also interesting to notice that the X-ray/IR delay from internal shocks is expected to scale with the mass of the central object (Malzac 2013). Thus, if the jet properties are similar between BHs and NSs, we expect a lag associated to the jet of ≈ 10 ms. Our observations set an upper limit to this lag of ≈ 60 ms (i.e. half the time resolution of the CCF). This scenario can be tested with higher time resolution IR instruments (see e.g. ERIS@VLT; Davies et al. 2018).

Another scenario which has been invoked to explain the O-IR flux excess in the hard state, is the production of cyclo-synchrotron radiation from an extended hot inflow (Veledina et al. 2011, 2013). According to these models, the X-rays would be then produced by the Comptonization of these photons (Wardziński & Zdziarski 2000; Poutanen & Vurm 2009). The sign of the lag, seems to suggest that Comptonization may be involved. Depending on the energy distribution of the electrons and/or the variability of some parameters of the system, a positive correlation with an O-IR lead can be reproduced (Poutanen & Vurm 2009; Veledina et al. 2017; Paice et al. 2021).

In the following paragraphs, we discuss the possible implications regarding a cyclo-synchrotron emitting region. These calculations need the value of the IR luminosity, which depends on distance and extinction. Regarding the distance, we will use the value obtained through photospheric radius expansion burst measurements (i.e. $\approx$ 5 kpc; Galloway et al. 2003). The extinction is more uncertain as there is no direct measurement of the $N_{\rm H}$. For the spectral analysis, we found a good fit using 1.35×10^{22} cm^2 (see Table 1), however past works have also found good fits using a higher $N_{\rm H}$ (roughly by a factor of 2). Using the relation found by Güver & Özel (2009) such values of $N_{\rm H}$ lead to A_V ranging between $\approx$6 and 11. Following Cardelli, Clayton & Mathis (1989) law, these in turn translate into A_K between ≈ 0.7 and 1.3. For our calculations we kept consistent with our spectral fit, and adopted the lower value of A_K. We caution, however, that the discussed values may change by a factor of a few depending on the extinction.

If the IR emission coincides with the peak of the cyclotron spectrum, it is possible to constrain the geometry of the emitting region. In details, adapting the equations described in Masters et al. (1977) for accreting white dwarfs, the radius of a slab emitting cyclotron radiation can be written as:

$$R = \sqrt{\frac{12c^2}{32\pi^2}\frac{L_{\rm cyc}}{kT\nu^3}} \quad (1)$$

where $L_{\rm cyc}$ is the observed luminosity at the electromagnetic frequency ν (1.5×10^{14} Hz), and T is the temperature of the slab. The exact temperature of the cyclotron emitting region is not known. However, we can assume that its temperature will not be higher than the coronal temperature inferred from the X-ray spectral fit ($kT_{\rm e} \approx 15$ keV). Therefore, this will give us a lower limit to the radius. We note that this is valid under the assumption of a thermal Maxwellian distribution for the electrons, and the value of the effective temperature could change depending on the energy distribution of the electrons. We obtain a de-reddened K_S band luminosity $L_{\rm cyc}$ of $\approx 10^{33}$ erg s^{-1}; given, however given an IR rms of approximately few percent, the luminosity of the variable component (responsible for the CCF) could be lower as $\approx 10^{31}$ erg s^{-1}. By plugging in these values in equation (1), we find that R has to be at least of the order of 10^8–10^9 cm. Such values seem unlikely, as they would be marginally consistent with the light travel time distance between the X-ray and the IR emitting region ($\approx 10^{-2}$ light seconds, i.e. 10^8 cm).

We also considered the case of an IR emitting synchrotron region. In detail, similarly to Chaty et al. (2011), we used a one-zone cylindrical region emitting IR synchrotron radiation. Although a more realistic description should include a stratified hot flow (Veledina, Poutanen & Vurm 2013), we adopt this approximation as it allows us to find a relatively simple relation between the fundamental quantities such as radius (R) and height of the slab (h), magnetic field (B), break of the synchrotron radiation, and flux. Thus, we can constrain the parameters of the system as well as the geometry of the corona. In details, assuming equipartition ($\xi = 1$), and the distance of 4U 1728−34, equations 1 and 2 from Chaty et al. (2011) can be written as follows:

$$B = C_B \nu \left(\frac{h}{S}\right)^{\beta} \text{ [G]} \quad (2)$$

$$R = \frac{C_R}{\nu}\left(\frac{S}{h}\right)^{\alpha} \text{ [cm]} \quad (3)$$

where ν is the break of the synchrotron spectrum expressed in units of 10^{14} Hz, S is the flux in units of 10 mJy, h is the height expressed in units of R (i.e. H/R), while C_R and C_B are constants (respectively, 2.5×10^8 and 5×10^5). The values of the indices α and β are, respectively, 17/36 and 1/9.

Díaz Trigo et al. (2018) measured the broad-band spectral energy distribution of 4U 1728−34 in a similar spectral state, finding a break frequency between $1.3 - 11.0 \times 10^{13}$ Hz ($\nu \approx 1.3 - 11.0 \times 10^{-1}$). Moreover, given the sign of the lag it is implausible that most of the variability arises from the jet. Thus, we can assume that the height of the cylinder is smaller than the radius (i.e. $h_{\rm max} = 1$). Finally, given a rms of a few percent, we can place a lower limit to the (variable) synchrotron flux of $\approx 10^{-2}$ mJy ($S_{\rm min} \approx 10^{-3}$). By combining these three quantities we can constrain the magnetic field and radius of the

slab. For the former, this translates into:

$$B < B_{\rm max} = C_B \nu_{\rm max} \left(\frac{h_{\rm max}}{S_{\rm min}}\right)^{\beta} \approx 10^6\,{\rm G} \quad (4)$$

Such a value is in line with the expectations from weakly magnetized sources, such as 4U 1728−34 (see e.g. Casella et al. 2008; Ludlam et al. 2019). When considering the radius, instead, we obtain:

$$R > R_{\rm min} = \frac{C_R}{\nu_{\rm max}} \left(\frac{S_{\rm min}}{h_{\rm max}}\right)^{\alpha} \approx 9 \times 10^6\,{\rm cm} \quad (5)$$

Such a value is consistent with the value inferred through our X-ray spectral fitting ($R_{in} = 5 - 19 \times 10^6$ cm). Thus, if we now consider the upper limit placed by the *NuSTAR* data analysis (i.e. fixing $R = R_{\rm max} = 1.9 \times 10^7$ cm) we can also rearrange the equations and place constraints on $h_{\rm min}$ and $\nu_{\rm min}$. Regarding h we obtain:

$$h > h_{\rm min} = \left(\frac{C_R}{\nu_{\rm max} R_{\rm max}}\right)^{\frac{1}{\alpha}} S_{\rm min} \approx 0.2 \quad (6)$$

which would point towards a thick wedge. We note that recent X-ray polarimetric measurements on other low magnetic field NS LMXBs at higher accretion rates have pointed towards a spherical geometry, with a smaller truncation radius (Capitanio et al. 2023; Chatterjee et al. 2023; Farinelli et al. 2023). Thus, the lack of fast IR stochastic variability in the soft states (Vincentelli et al. 2020) could be explained with a contracting hot flow as the source approaches higher accretion rates (see e.g. Esin et al. 1997; Wijnands & van der Klis 1999; Ingram & Done 2010; Muñoz-Darias et al. 2014; van den Eijnden et al. 2020). More data of these sources with both fast multiwavelength timing and polarimetric observations may thus be used in the future to place stronger constraints on the evolution of this component as a function of luminosity.

Regarding the synchrotron break we obtain:

$$\nu > \nu_{\rm min} = \frac{C_R}{R_{\rm max}} \left(\frac{S_{\rm min}}{h_{\rm max}}\right)^{\alpha} \approx 0.5 \quad [\times 10^{14}\,{\rm GHz}] \quad (7)$$

This is consistent with the results obtained by Díaz Trigo et al. (2018) and suggests that the turn-over between optically thin and optically thick region is in the near-IR band. New multiwavelength observations, with mid-IR coverage are required to confirm this scenario.

4.2 Type-I burst

We have measured for the second time the delayed IR counterpart of an X-ray type-I burst in 4U 1728−34. It is generally accepted that these X-ray flashes occur because of a thermonuclear runway on the surface of the accreting NS (Hansen & van Horn 1975; Woosley & Taam 1976). The presence of UV/O/IR counterparts in these systems is usually interpreted as reprocessing from the outer disc and the companion star (O'Brien et al. 2002; Hynes et al. 2006).

Interestingly, we found a variation in the X-ray/IR delay, passing from 4.5 to 7.2 s compared to a previous observation (Vincentelli et al. 2020). Such a marked difference suggests that the IR burst originates from thermal reprocessed emission of the donor star. If this is due only to a change in the orbital phase (i.e. the change of hot inflow geometry does not affect the delay between the driving and reprocessed burst), this measurement can be used to further constrain the period of the system and put a limit on the inclination.

4.2.1 *Geometrical interpretation: limits on the orbital period*

Similarly, to Vincentelli et al. (2020), by simply considering the donor star as a point source and assuming that the 7.2 s is measured at superior conjunction with $i = 90°$, we can set a lower limit to the orbital period. In that case the delay (τ) would correspond to $\tau = 2a/c$ (where a is the orbital separation and c is the speed of light), plus the reprocessing time (which is expected to be less than a few 100 ms; Cominsky, London & Klein 1987). Even considering a more realistic case, where the star occupies a significant fraction of the orbital separation, or if the IR emission arises from a large fraction of the star, this limit would still hold. Thus, given a delay of 7.2 s, we can say that $a = 3.5c$. According to Kepler's third law (for a canonical NS mass of 1.4 $M_\odot$), this yields a minimum orbital period ≈ 3 h, ruling out the ultra-compact nature of the source proposed by Galloway et al. (2010). This would also be in line with the period derived from recent transient pulsations searches ($P_{\rm orb}$ between 2 and 8 h; Bahar, Chakraborty & Göğüş 2021).

4.2.2 *Geometrical interpretation: limits on the inclination*

Under the hypothesis that the IR burst arises from reprocessing, the measurement of the delays from two different events can be used to put the first lower limit to the inclination of the source. The light travel time distance between the central and donor star in an orbiting system with a semimajor axis a, with an inclination i at an orbital phase ϕ is (O'Brien et al. 2002):

$$\tau = \frac{a}{c} \cdot [1 + \sin i \cdot \cos \phi] \quad (8)$$

Thus, if we have two bursts of the same system measured at different phases, we will observe a difference in the lag between the driving and reprocessed burst. We can express the difference between the measured reprocessed lags as:

$$\Delta\tau = \tau_2 - \tau_1 = \frac{a}{c} \sin i \cdot [\cos \phi_2 - \cos \phi_1] \quad (9)$$

For a given inclination, the maximum observable time difference between two delays will be seen when the phases of the two bursts are 0 and π, thus:

$$\Delta\tau < \frac{2a_{\rm max}}{c} \sin i \quad (10)$$

By assuming a maximum $a_{\rm max}/c = 10$ (i.e. the value of semimajor axis for an orbital period of ≈ 20 h[4]), this gives $i > 8°$. This is consistent with previous modelling of the source (Vincentelli et al. 2020) and sets the first geometrical constraint on the inclination of 4U 1728−34.

4.2.3 *Additional effects*

It is interesting to notice that the observed IR burst shows also some properties that are not fully consistent with the reprocessing scenario. Its duration is significantly shorter than that of the X-ray burst, and the shape does not fully resemble the observed one at high energy (opposite to the soft state case; Vincentelli et al. 2020). The shorter duration could be explained by assuming a high continuum level (see e.g. Vincentelli et al. 2020) and that we observe only a small fraction of the star reprocessing the X-rays (i.e. if the star is between

[4]The maximum orbital period which can be sustained with a stable outburst according to the disc-instability model for 4U1728−34's mass accretion rate is ≈10–20 h (Dubus et al. 2019).

us and the NS; O'Brien et al. 2002). A different reprocessed burst profile, however, could also arise if the burst observed by the outer regions of the system is different from the observed X-ray burst. A possible explanation for this could come from the effect of an extended hot flow, which is present during this state (a similar argument has been invoked also to explain the lack of correlation between AGN X-ray and optical/UV lightcurves; see e.g. Gardner & Done 2017). For example, if the corona is depleted during the type-I burst (as suggested by high energy observations and simulations) and reappears during its decay, it may scatter the X-ray flux in a complex way, partially obscuring the NS surface to the companion. This would lead to a 'truncated' driving signal, explaining the different shape of the reprocessed burst.

An additional signature of the corona is the presence of a marginal 'dip' in the IR lightcurve at the peak of the X-ray burst. Further observations are required to confirm this feature; however, it is interesting to note that such an anticorrelation would be expected if the IR arose from synchrotron radiation by the corona (Degenaar et al. 2018). If the corona cools down due to the dramatic increase of soft seed photons from the thermonuclear flash (as supported by high energy observations of type-I X-ray bursters; see e.g. Maccarone & Coppi 2003; Chen et al. 2013; Ji et al. 2013, 2014a,b; Kajava et al. 2017; Chen et al. 2018; Sánchez-Fernández et al. 2020), then the synchrotron radiation is also expected to then the synchrotron radiation is also expected to drop. Consolidation of this dip with further observations may lead to new independent constraints on the evolution of the accretion flow during these extreme events.

5 CONCLUSIONS

We have performed the first simultaneous, sub-second IR/X-ray observations of an accreting NS in the low hard state. We found two main results:

(i) We discovered a correlated signal between X-ray and infrared on millisecond time-scales with an IR lead of $\approx$ 30–40 ms. There are no specific models that can explain this feature. However, given the energy dependence of the lag, we propose a scenario in which IR cyclotron or (more likely) synchrotron photons are produced by an extended hot inflow, and then Comptonized by the more energetic electrons responsible for the X-ray non-thermal emission.

(ii) We detected the IR counterpart of a type-I burst with lag of $\approx$ 7.2 s with respect to the X-ray one. By combining this result with past measurements, and assuming that the change is not affected by the spectral state, we obtain a minimum orbital period of $\approx$ 3 h and a lower limit to the inclination of $\approx 8^\circ$. However, we also note that the shape of the IR burst suggests that some interaction with the corona is at play.

These results confirm the strength of fast multiwavelength variability for studying accretion processes. Moreover, the discovery of correlated X-ray/IR sub-second variability 4U 1728−34 opens a new window in the study of NS LMXBs. Further observations with new IR instruments with higher time resolution (e.g. ERIS@VLT; Davies et al. 2018) may be able to resolve the observed peak in the CCF, leading to unprecedented constraints on the geometry of the accretion flow and jet's physical conditions in NS LMXBs.

ACKNOWLEDGEMENTS

We thank the referee for the valuable comments which improved the quality and readability of the paper. This work benefited from the discussions done during the ISSI meeting in Bern ''Looking at the disc-jet coupling from different angles''. FMV acknowledges support from the grant FJC2020-043334-I financed by MCIN/AEI/10.13039/501100011033 and Next Generation EU/PRTR. This work is supported by the Spanish Ministry of Science under grants PID2020–120323GB–I00, PID2021–124879NB-I00, and EUR2021–122010'. MB acknowledges financial contribution from grant PRIN-INAF 2019 no. 15. YC acknowledges support from the grant RYC2021-032718-I, financed by MCIN/AEI/10.13039/501100011033 and the European Union NextGenerationEU/PRTR. LS acknowledges financial contributions from ASI-INAF agreements 2017-14-H.O and I/037/12/0; from 'iPeska' research grant (PI Andrea Possenti) funded under the INAF call PRIN-SKA/CTA (resolution 70/2016), from PRIN-INAF 2019 no. 15 and from the Italian Ministry of University and Research (MUR), PRIN 2020 (prot. 2020BRP57Z) "GEMS".

This research has made use of the VizieR catalogue access tool, CDS, Strasbourg, France (DOI: 10.26093/cds/vizier). The original description of the VizieR service was published in 2000, A&AS 143, 23.

DATA AVAILABILITY

All raw data are publically available on the online repositories of the ESO, *XMM-Newton*, and *NuSTAR* archives.

REFERENCES

Altamirano D., van der Klis M., Méndez M., Jonker P. G., Klein-Wolt M., Lewin W. H. G., 2008, ApJ, 685, 436
Armas Padilla M., Ueda Y., Hori T., Shidatsu M., Muñoz-Darias T., 2017, MNRAS, 467, 290
Baglio M. C., D'Avanzo P., Campana S., Goldoni P., Masetti N., Muñoz-Darias T., Patiño-Álvarez V., Chavushyan V., 2016, A&A, 587, A102
Baglio M. C. et al., 2019, A&A, 631, A104
Baglio M. C. et al., 2023, A&A, preprint (arXiv:2305.14509)
Bahar Y. E., Chakraborty M., Göğüş E., 2021, PASA, 38, e011
Belloni T., Homan J., Casella P., van der Klis M., Nespoli E., Lewin W. H. G., Miller J. M., Méndez M., 2005, A&A, 440, 207
Belloni T. M., Motta S. E., Muñoz-Darias T., 2011, Bull. Astron. Soc. India, 39, 409
Burke M. J., Gilfanov M., Sunyaev R., 2017, MNRAS, 466, 194
Buxton M. M., Bailyn C. D., Capelo H. L., Chatterjee R., Dinçer T., Kalemci E., Tomsick J. A., 2012, AJ, 143, 130
Capitanio F. et al., 2023, ApJ, 943, 129
Cardelli J. A., Clayton G. C., Mathis J. S., 1989, ApJ, 345, 245
Casella P., Altamirano D., Patruno A., Wijnands R., van der Klis M., 2008, ApJ, 674, L41
Casella P. et al., 2010, MNRAS, 404, L21
Chatterjee R., Agrawal V. K., Jayasurya K. M., Katoch T., 2023, MNRAS, 521, L74
Chaty S., Dubus G., Raichoor A., 2011, A&A, 529, A3
Chen Y.-P., Zhang S., Zhang S.-N., Ji L., Torres D. F., Kretschmar P., Li J., Wang J.-M., 2013, ApJ, 777, L9
Chen Y. P. et al., 2018, ApJ, 864, L30
Cominsky L. R., London R. A., Klein R. I., 1987, ApJ, 315, 162
Corbel S., Fender R. P., 2002, ApJ, 573, L35
Corbel S. et al., 2013, MNRAS, 431, L107
D'Aí A. et al., 2006, A&A, 448, 817
Davies R. et al., 2018, in Evans C. J., Simard L., Takami H.eds, SPIE Conf. Ser., Vol. 10702, Ground-based and Airborne Instrumentation for Astronomy VII. SPIE, Bellingham, p. 1070209
De Marco B. et al., 2017, MNRAS, 471, 1475
Degenaar N. et al., 2014, ApJ, 784, 122
Degenaar N. et al., 2018, Space Sci. Rev., 214, 15
Dhillon V. S. et al., 2007, MNRAS, 378, 825

Díaz Trigo M. et al., 2018, A&A, 616, A23
Done C., Gierliński M., Kubota A., 2007, A&AR, 15, 1
Dubus G., Kern B., Esin A. A., Rutledge R. E., Martin C., 2004, MNRAS, 347, 1217
Dubus G., Done C., Tetarenko B. E., Hameury J.-M., 2019, A&A, 632, A40
Durant M. et al., 2011, MNRAS, 410, 2329
Eastman J., Siverd R., Gaudi B. S., 2010, PASP, 122, 935
Esin A. A., McClintock J. E., Narayan R., 1997, ApJ, 489, 865
Farinelli R. et al., 2023, MNRAS, 519, 3681
Fender R. P., Belloni T. M., Gallo E., 2004, MNRAS, 355, 1105
Galloway D. K., Psaltis D., Chakrabarty D., Muno M. P., 2003, ApJ, 590, 999
Galloway D. K., Yao Y., Marshall H., Misanovic Z., Weinberg N., 2010, ApJ, 724, 417
Gandhi P. et al., 2008, MNRAS, 390, L29
Gandhi P. et al., 2010, MNRAS, 407, 2166
Gandhi P. et al., 2011, ApJ, 740, L13
Gandhi P. et al., 2017, Nat. Astron., 1, 859
García J. et al., 2014, ApJ, 782, 76
Gardner E., Done C., 2017, MNRAS, 470, 3591
Gierliński M., Done C., Page K., 2009, MNRAS, 392, 1106
Güver T., Özel F., 2009, MNRAS, 400, 2050
Hansen C. J., van Horn H. M., 1975, ApJ, 195, 735
Harrison F. A. et al., 2013, ApJ, 770, 103
Hasinger G., van der Klis M., 1989, A&A, 225, 79
Homan J. et al., 2007, ApJ, 656, 420
Hynes R. I., 2005, ApJ, 623, 1026
Hynes R. I. et al., 2006, ApJ, 651, 401
Ingram A., Done C., 2010, MNRAS, 405, 2447
Jamil O., Fender R. P., Kaiser C. R., 2010, MNRAS, 401, 394
Ji L. et al., 2013, MNRAS, 432, 2773
Ji L., Zhang S., Chen Y. P., sZhang S. N., Kretschmar P., Wang J. M., Li J., 2014a, A&A, 564, A20
Ji L., Zhang S., Chen Y., Zhang S.-N., Torres D. F., Kretschmar P., Li J., 2014b, ApJ, 782, 40
Kajava J. J. E., Sánchez-Fernández C., Kuulkers E., Poutanen J., 2017, A&A, 599, A89
Kalamkar M., Casella P., Uttley P., O'Brien K., Russell D., Maccarone T., van der Klis M., Vincentelli F., 2016, MNRAS, 460, 3284
Kalemci E., Kara E., Tomsick J. A., 2022, in, Bambi C., Santangelo A., eds, Handbook of X-ray and Gamma-ray Astrophysics. Springer, Singapore, p. 9
Kanbach G., Straubmeier C., Spruit H. C., Belloni T., 2001, Nature, 414, 180
Kong A. K. H., Charles P. A., Kuulkers E., 1998, New Astron., 3, 301
Kosenkov I. A., Veledina A., Suleimanov V. F., Poutanen J., 2020, A&A, 638, A127
Lin D., Remillard R. A., Homan J., 2007, ApJ, 667, 1073
Lin D., Remillard R. A., Homan J., 2009, ApJ, 696, 1257
Ludlam R. M. et al., 2019, ApJ, 873, 99
Maccarone T. J., Coppi P. S., 2003, A&A, 399, 1151
McGowan K. E., Charles P. A., O'Donoghue D., Smale A. P., 2003, MNRAS, 345, 1039
Malzac J., 2013, MNRAS, 429, L20
Malzac J., 2014, MNRAS, 443, 299
Marino A. et al., 2020, MNRAS, 498, 3351
Masters A. R., Pringle J. E., Fabian A. C., Rees M. J., 1977, MNRAS, 178, 501
Méndez M., Karpouzas K., García F., Zhang L., Zhang Y., Belloni T. M., Altamirano D., 2022, Nat. Astron., 6, 577
Migliari S., Fender R. P., 2006, MNRAS, 366, 79
Migliari S. et al., 2010, ApJ, 710, 117
Motch C., Ilovaisky S. A., Chevalier C., 1982, A&A, 109, L1
Motch C., Ricketts M. J., Page C. G., Ilovaisky S. A., Chevalier C., 1983, A&A, 119, 171
Muñoz-Darias T., Martínez-Pais I. G., Casares J., Dhillon V. S., Marsh T. R., Cornelisse R., Steeghs D., Charles P. A., 2007, MNRAS, 379, 1637
Muñoz-Darias T., Fender R. P., Motta S. E., Belloni T. M., 2014, MNRAS, 443, 3270
O'Brien K., Horne K., Hynes R. I., Chen W., Haswell C. A., Still M. D., 2002, MNRAS, 334, 426
Paice J. A. et al., 2019, MNRAS, 490, L62
Paice J. A. et al., 2021, MNRAS, 505, 3452
Papitto A. et al., 2019, ApJ, 882, 104
Peterson B. M., Wanders I., Horne K., Collier S., Alexander T., Kaspi S., Maoz D., 1998, PASP, 110, 660
Piraino S., Santangelo A., Kaaret P., 2000, A&A, 360, L35
Pirard J.-F. et al., 2004, in Moorwood A. F. M., Masanori I., eds, Proc. SPIE Conf. Ser., Vol. 5492, Ground-based Instrumentation for Astronomy. SPIE, Bellingham, p. 1763
Poutanen J., Vurm I., 2009, ApJ, 690, L97
Poutanen J., Veledina A., Revnivtsev M. G., 2014, MNRAS, 445, 3987
Press W. H., 1978, Comments Astrophys., 7, 103
Psaltis D., Belloni T., van der Klis M., 1999, ApJ, 520, 262
Russell D. M., Fender R. P., Hynes R. I., Brocksopp C., Homan J., Jonker P. G., Buxton M. M., 2006, MNRAS, 371, 1334
Russell D. M., Fender R. P., Jonker P. G., 2007, MNRAS, 379, 1108
Sánchez-Fernández C., Kajava J. J. E., Poutanen J., Kuulkers E., Suleimanov V. F., 2020, A&A, 634, A58
Scaringi S. et al., 2015, Sci. Adv., 1, e1500686
Shahbaz T. et al., 2015, MNRAS, 453, 3461
Shahbaz T., Dallilar Y., Garner A., Eikenberry S., Veledina A., Gandhi P., 2018, MNRAS, 477, 566
Shahbaz T. et al., 2023, MNRAS, 520, 542
Shaposhnikov N., Titarchuk L., Haberl F., 2003, ApJ, 593, L35
Strüder L. et al., 2001, A&A, 365, L18
Tananbaum H., Gursky H., Kellogg E., Giacconi R., Jones C., 1972, ApJ, 177, L5
Tetarenko B. E., Lasota J. P., Heinke C. O., Dubus G., Sivakoff G. R., 2018, Nature, 554, 69
Tetarenko A. J. et al., 2021, MNRAS, 504, 3862
Uttley P., McHardy I. M., Vaughan S., 2005, MNRAS, 359, 345
Uttley P., Cackett E. M., Fabian A. C., Kara E., Wilkins D. R., 2014, A&AR, 22, 72
van den Eijnden J. et al., 2020, MNRAS, 493, 1318
van der Klis M., 1994, ApJS, 92, 511
van der Klis M., 2006, in Lewin W., van der Klis M., eds, Cambridge Astrophysics Series, Vol. 39, Rapid X-ray Variability In: Compact stellar X-ray sources. Cambridge Univ. Press, Cambridge, p. 39
Vaughan S., Edelson R., Warwick R. S., Uttley P., 2003, MNRAS, 345, 1271
Veledina A., Poutanen J., Vurm I., 2011, ApJ, 737, L17
Veledina A., Poutanen J., Vurm I., 2013, MNRAS, 430, 3196
Veledina A., Gandhi P., Hynes R., Kajava J. J. E., Tsygankov S. S., Revnivtsev M. G., Durant M., Poutanen J., 2017, MNRAS, 470, 48
Vincentelli F. M. et al., 2018, MNRAS, 477, 4524
Vincentelli F. M. et al., 2019, ApJ, 887, L19
Vincentelli F. M., Cavecchi Y., Casella P., Migliari S., Altamirano D., Belloni T., Diaz-Trigo M., 2020, MNRAS, 495, L37
Vincentelli F. M. et al., 2021, MNRAS, 503, 614
Vincentelli F. M. et al., 2023, Nature, 615, 45
Wang Y., Méndez M., Sanna A., Altamirano D., Belloni T. M., 2017, MNRAS, 468, 2256
Wang Y. et al., 2019, MNRAS, 484, 3004
Wardziński G., Zdziarski A. A., 2000, MNRAS, 314, 183
Wijnands R., van der Klis M., 1999, ApJ, 514, 939
Woosley S. E., Taam R. E., 1976, Nature, 263, 101
Yan Z., Yu W., 2015, ApJ, 805, 87
Zdziarski A. A., Gierliński M., 2004, Prog. Theor. Phys. Suppl., 155, 99
Zdziarski A. A., Szanecki M., Poutanen J., Gierliński M., Biernacki P., 2020, MNRAS, 492, 5234
Zdziarski A. A., Tetarenko A. J., Sikora M., 2022, ApJ, 925, 189

This paper has been typeset from a TEX/LATEX file prepared by the author.